All-Nanoparticle Monolayer Broad-Band Anti-Reflective and Self-Cleaning Transparent Glass Coating

Alexey Gruzd,[†] Alexander Tokarev,[†] Igor Tokarev[††], Dmitri Kuksenkov[§], and Sergiy Minko[†,]**

[†] Nanostructured Materials Lab, University of Georgia, Athens, GA 30602, USA

[††] Eastman Chemical Company, Kingsport, TN, 37660 USA

[§] Sullivan Park Science & Technology Center, Corning Incorporated, Corning, NY14831, USA

*Corresponding authors: KuksenkoDV@Corning.com; sminko@uga.edu

KEYWORDS: antireflective coatings, nanostructured optical surfaces, transparent surfaces, spray coating, silica particles

ABSTRACT:

The vast majority of LED and LCD displays, solar panels, and windows in residential and industrial buildings use glass panels owing to their high mechanical stability, chemical resistance, and optical properties. Glass surfaces reflect about 4-5% of incident light if no antireflective coating is applied. In addition to energy losses in displays, surface reflections diminish picture quality. Engineering of antireflective coatings can be beneficial for all types of glass screens, specifically for large screens and touch-screen devices when scratch-resistance and self-cleaning properties of the glass surface are also desired. A scalable and robust approach to produce antireflective coatings for glass surfaces with desired optical and mechanical properties is introduced in this work. The developed coating mimics the structure of a moth-eye cornea. The coating is a subwavelength microstructured thin layer on the glass surface made of a monolayer of hemispherical silica nanoparticles obtained by hydrothermal fusion of spherical particles to the glass substrate. The sequence of the particle deposition in the layer-by-layer process is adjusted to balance attractive-repulsive interactions among nanoparticles and between the nanoparticles and the glass surface to generate coatings with a high surface coverage, up to 70%, which exceeds 54.7% limit of the random sequential addition model. This level of surface coverage allows for a combination of properties beneficial for the described applications: (i) an average reflectance of

0.5±0.2% for visible and near-infrared optical spectrum, (ii) an improved mechanical stability and scratch resistance, and (iii) non-wetting behavior.

Introduction

Antireflective (AR) coatings that subdue the light reflection of substrates are continuously attracting considerable attention due to their practical benefits for a wide range of optical and optoelectronic devices, such as optical lenses, displays, solar panels, light moduli, anti-glare glass surfaces, etc.[1-5] The light reflection of a flat glass surface in contact with air is about 4-5 %. For both sides of the glass-air interface, the reflected light energy approaches 8-10 %. Direct outcomes of an AR coating are improved efficiency of optical devices due to reduction of energy loss, minimized parasitic glare, and improved quality of the picture. Many efforts have been made to combine AR properties with additional functional properties, such as scratch-resistance, self-cleaning, anti-fog, antimicrobial, to name a few.

There are two common concepts to design AR coatings. The first approach is based on one-layer or multilayer structures with adjusted thicknesses and refractive indices that result in destructive interference of the reflected light. A traditional quarter-wave layer coating is a low-cost approach to achieve total transmittance for a particular wavelength. However, for a broadband-light, such a one-layer technique is less efficient. Multilayer AR coatings are much more efficient in a wide range of wavelengths.[6] The multilayer-coating technology is commonly used for small size optical devices, for example, optical lenses. Physical vapor deposition is typically used to form layers with controlled thicknesses and refractive indices. It remains challenging to extend this technology for broader applications because of a relatively high cost and substrate size limitations of the vapor deposition technique. A potential alternative to the conventional fabrication of multilayer coatings by physical vapor deposition is the sol-gel method.[7-13] However, a number of problems remain unsolved, including material selection to match optical and thermal expansion characteristics.

The second concept is to design an AR coating made of subwavelength structures that provide a gradual change of a refractive index at the interface between the glass substrate and air. Thin porous or textured structures with a normal to the glass surface gradient of the refractive index is a promising realization of this concept.[1, 14] This design was inspired by the texture of a night moth cornea that is comprised of nanosized conical omnidirectional broadband high-transmission structures.[14] The concept of transparent subwavelength coatings that mimic a moth cornea has been extensively explored using various deposition methods including reactive ion etching[15-18], soft and nanoimprint lithography[19-21], arraying polymer and silica nanostructures (by self-

assembly[22-25] and spin-coating[26]), and deposition of porous structures (using dip-coating,[27-29] spraying,[30-32] and sputter-coating[33]).

Consequently, nanostructured coatings combine advantages of one-layer AR coatings, including no need to optimize optical properties and match thermal expansion coefficients for two or more layers on the substrate and advantages of multilayer coatings, including broadband and wide-angle AR properties. The disadvantages of nanostructured monolayer coatings are associated with often quite complex fabrication methods and their binding to glass substrates and challenges in achieving durability.

Here, we introduce a facile and scalable approach to fabricate robust, transparent nanostructured AR coatings on glass substrates without using additional materials to strongly bind nanostructures to the glass surface. In this approach, a monolayer of silica nanoparticles is deposited on the glass surface via self-assembly and spray-coating techniques (**Figure 1**). Such a deposition procedure can be easily automated and adjusted to various dimensions and curvature of glass substrates. Afterward, silica particles are fused with the substrate to achieve a highly durable and chemically resistant nanostructured silica surface, which contains no organic materials. In this work, we developed novel methods to fabricate silica particle monolayers with a high surface coverage on the glass substrate which prevent 3D-aggregation of these particles and enable their binding to the glass surface using the hydrothermal fusion. The combination of these two methods results in the formation of densely packed monolayers of hemispherical nanostructures with AR properties and no inclusion of soft materials. The resulting glass surface with hemispherical nanoparticles mimics the moth-eye texture and provides broadband transparency. Compared to other reported methods, this approach is primarily focused on maintaining high AR properties, as well as mechanical stability, scratch resistance, and self-cleaning properties, while using a cost-efficient and scalable fabrication technique.

Experimental

Modeling of the optical properties

The modeling of optical properties in a wavelength range of 380-2250 nm was conducted using the Essential Macleod software package. The coatings were represented as a stack of sublayers with the corresponding porosity and chromatic dispersion, see Supporting Information (SI), **Figure S1**.

Materials and Chemicals

Alkali aluminosilicate glass (common for mobile devices due to its chemically-reinforced shatter-resistant properties) slides. a perfluoropolyether (PFPE) silane solution for hydrophobic/oleophobic surface treatment, and a potassium salt bath were supplied by Corning Incorporated (Corning, NY, U.S.). Monodispersed silica nanospheres AngstromSphere (200 nm in diameter with a standard deviation of <10%) were obtained from Fiber Optic Center Inc (New Bedford, MA, U.S.). Silica nanoparticles (SiO_2, 25 nm in diameter) were purchased from nanoComposix (San Diego, CA, U.S.). Poly(diallyldimethylammonium chloride) (PDDA, 20% wt. % in H_2O, M_w = 150,000 g/mol), poly(sodium 4-styrenesulfonate) (PSS, M_w = 70,000, powder), 1-octanol (99%), cetyl trimethylammonium bromide (CTAB, 98%), sodium hydroxide (pellets) were purchased from Sigma-Aldrich. 3-aminopropyltriethoxysilane (APTS, 99%) was obtained from ACROS Organics (Thermo Fisher Scientific). 1,1′,2,2′ - perfluorooctyltriethoxysilane (PFOTS) was obtained from Gelest Inc (Morrisville, PA, US).

Preparation of the antireflective coatings

In order to deposit a single monolayer of silica nanoparticles onto a glass substrate, a layer-by-layer (LbL) assembly technique was used. The LbL process was realized by two methods: dip-rinse and spray coating. Herein, the dip-rinse term is used to emphasize the importance of rinsing and drying the coating after each deposition of silica particles. The fabrication technique is schematically illustrated in **Figure 1**. Alkali aluminosilicate glass slides were used as substrates for the coatings. Before any treatment, the slides were cleaned in a chromic mixture overnight and then rinsed in deionized (DI) water and dried with nitrogen. The cleaned glass slides were coated with alternating layers of positively and negatively charged polyelectrolytes by dipping them in 1 wt. % aqueous PDDA and PSS solutions. Redundant polyelectrolytes were removed by rinsing in DI water. The dipping process was repeated 6-8 times with PDDA as the surface layer of the LbL film (SI). The $(PDDA\text{-}PSS)_7PDDA$ multilayer system provides a uniform positive charge on the glass surface for subsequent deposition of silica nanoparticles. The silica nanospheres were dispersed in sodium hydroxide aqueous solution (30 wt % silica particles). The dispersion was sonicated for 2-3 hours, while every 5-10 minutes, sodium hydroxide was dropwise added to maintain the pH at 9.5. In preliminary experiments, silica particle samples of different diameters in a range of 70-300 nm were tested for the surface coverage and a fusion process taking into account that the latter results in a decrease of the height, *h*, of the resulting structural features. The best optical properties of the coated glass substrates were achieved for the fusion of 200 nm spherical particles as predicted by optical modeling. This work discusses the experiments with 200 nm particles only.

For the dip-rinse method, the LbL modified substrates were dipped in 30% wt dispersion of silica nanoparticles for 5 min, followed by rinsing with NaOH/H_2O (pH 9) solution and then with DI water, and completed by drying with a nitrogen flow. This process was repeated 1-4 times to increase the surface coverage by silica particles. In order to partially screen the negative charge of the deposited silica particles, the substrate was also immersed in an aqueous mixture of 1% octanol and 0.01% CTAB for 5 min with the subsequent rinsing with DI water, ethanol, DI water, and then dried with an N_2 flow. The mechanism behind the CTAB-octanol effect on the surface coverage is discussed in the Results and Discussion section.

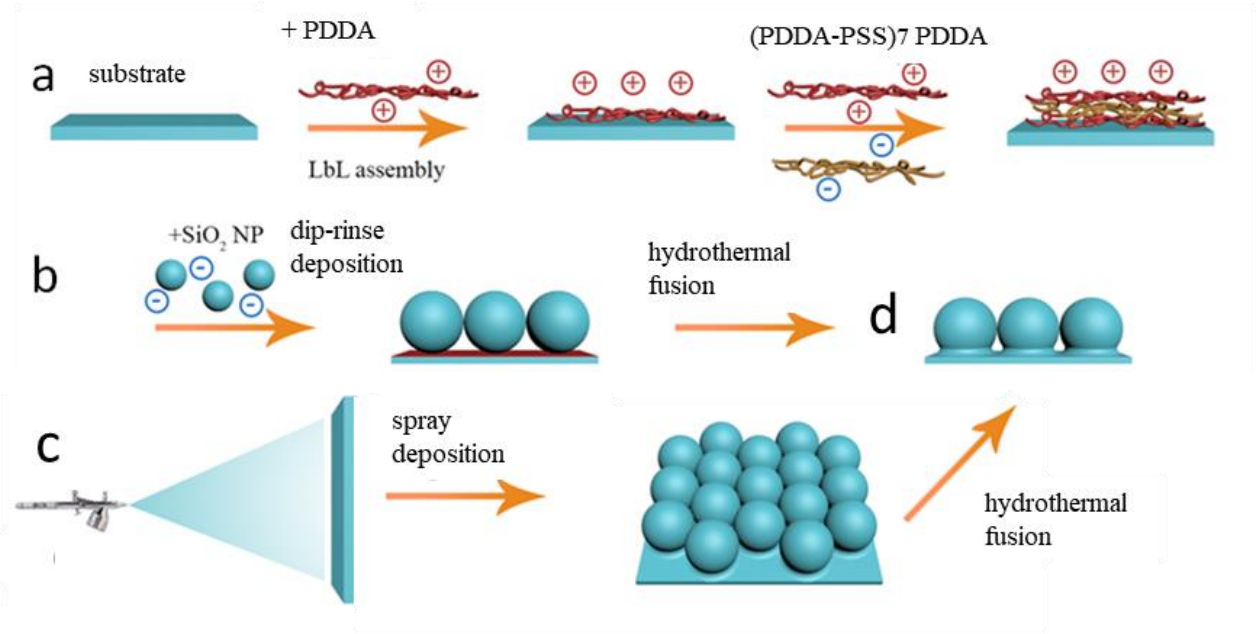

Figure 1. Schematic of the fabrication process of antireflective coatings: (a) LbL deposition of a polyelectrolyte anchoring layer, LbL silica particle deposition either by (b) dip-rinse or (c) spray method, and (d) hydrothermal annealing of the coating.

For the spray-coating method, the same solutions were deposited using an Airbrush kit instead. A typical spraying time was about 1 min with a liquid flow rate of 0.5-2 ml/min, an air pressure of 0.5 bar, and a distance of 50 mm (SI). Relative humidity in the deposition chamber was maintained at 15% at room temperature. Rinsing and drying were also performed with an Airbrush for 2 min for both washing and drying steps. The critical part of the spray-coating approach is to rinse the substrate immediately after the deposition solution is consumed to avoid drying of the redundant dispersion.

The deposited silica particles were fused with the alkali aluminosilicate glass substrate via hydrothermal annealing. For this purpose, the samples were treated in a furnace with a controlled steam flow. The time of treatment, temperature, and steam content were varied to achieve optimal

optical characteristics. The typical annealing temperature was 600 °C, the annealing time was 1 h, and about 100% water vapor atmosphere inside the furnace. At this temperature, all the organic components of the LbL anchoring layer were pyrolyzed and removed from the coating. A thorough analysis was performed to investigate the influence of annealing parameters on the coating structure and their effect on its optical characteristics. Details of this analysis are the subject of a separate study, and the results will be published elsewhere. After the annealing, the resulting glass substrates were additionally modified via an anion-exchange process by immersing the substrate in a molten potassium salt bath at 400 °C to secure mechanical characteristics of the glass (standard procedure for chemically strengthened glass production).

Preparation of self-cleaning antireflective coatings

For achieving self-cleaning properties, 0.01% wt. silica particles in aqueous dispersion (25 nm SiO_2; pH 10.5) were amino-functionalized with APTS (3 mM solution in water). This step was used to bind cationic functional groups to the surface of 25 nm silica particles, which provide electrostatic interaction and hydrogen bonding with the surface of silica particles in the antireflective coating. The amino-functionalized particles were sprayed on top of the 200 nm particle coating. The substrates were then cleaned by plasma treatment for 2 min to degrade all the organic materials on the surface of the coating. Finally, the samples were functionalized using a 1% toluene solution of PFOTS overnight. Afterward, the treated substrates were rinsed with toluene and ethanol and then dried with nitrogen.

Characterization of the antireflective coatings

The morphology of the obtained self-assembled monolayers of silica nanoparticles was characterized by a JEOL 7400 high-resolution field-emission scanning electron microscope (FE-SEM) using pristine samples without gold coating. A surface coverage with nanoparticles was estimated as a ratio of the projected area of silica particles to the total area of the underlying substrate (Figure S2a-c). FE-SEM imaging was adjusted to avoid glowing effects due to surface charging. The particle size correlates with that measured by SEM and AFM (Figure S2d). The image processing was performed using the Gwyddion software (Figure S3).

A Zeta-potential for the functionalized glass surfaces was estimated with a ZetaSpin system (Carnegie Mellon University) using 2.5 cm disk-shaped samples in 0.2 M NaCl aqueous solutions (Figure S4).

Transparency and haze were measured with a HazeGard instrument and a UV-2401PC spectrophotometer. Reflection measurements were performed using a Filmetrics F40 microscope

attachment to a Nikon optical microscope in a spectral range from 300 to 800 nm. The transmittance was measured in several locations to ensure the optical homogeneity of the samples.

The mechanical stability of the samples was characterized by the standard pencil scratch test with pencil hardnesses up to 6H. The test method is fully described in ASTM D3363-92a. Additionally, the samples were tested by a steel wool scratch test with controlled pressure.

Results and Discussion

Structural design

According to a simple model[1], for glass substrates with a refractive index of 1.5, the ideal refractive index of a single-layer quarter-wave coating is $n_o = (n_a n_g)^{1/2} = (1 \cdot 1.5)^{1/2} = 1.229$ and the optimal layer thickness is $d_o = \lambda/(4n_o) = 550 \text{ nm}/(4 \cdot 1.229) = 112$ nm, where n_a and n_g are the refractive indices of air and the glass at the source wavelength of 550 nm. No solid materials are available with such a refractive index. A possible solution is to prepare a porous structure, for example, by deposition of a monolayer of solid particles (Figure 2), when the refractive index could be tuned by a change in surface coverage and shape of nanostructures. For spherical particles, the optimal refractive index $n_o = 1.229$ is approached at a surface coverage of about 76.5% (51% volume porosity). However, such a surface coverage is not possible by a random particle deposition process. For the hexagonally packed spherical particles in a monolayer configuration (Figure 2c), the surface coverage reaches 90%, while for random deposition (Figure 2f), it is not greater than 60%. Another important aspect is the particle adhesion to the substrate, which is greater for hemispherical particles (Figure 2 a,b) and minimal for spheres.

In addition to the effective refractive index and adhesion, the shape of submicron particles is very important to approach a low average reflectivity for a wide spectral range and a wide range of angles of incidence. It was shown with simulations and experiments[34-35] that a semi-conical profile that mimics the moth-eye cornea structure (Figure 2e) is the most efficient AR microstructure for minimized broadband and wide-angle reflectance. Approaching such a profile requires a complex lithographic manufacturing technology. Among various proposed types of AR subwavelength structures,[35] a monolayer of hemispheres (Figure 2 a,b) on a plane substrate (glass) is selected for this work because of the gradual change of effective refractive index across the coating and the largest particle-substrate contact area to improve the mechanical stability of the coating. The profile of a gradual decrease of a refractive index from glass to air depends on the packing of hemispheres. The refractive index profile becomes less steep as the packing density is increased (**Figure 2a,b),** which is in stark contrast to the case of spherical particles when, even for a densely

packed monolayer, a sharp spike of the refractive index at the interface between the particles and substrate could result in an increased reflectance of the coating (**Figure 2c**).

Consequently, the structure of densely packed hemispheres is a preferential structure. Such a structure could be obtained using lithography. In this work, we found that a hydrothermal fusion of spherical silica particles with the glass substrate led to structures that resembled both an array of hemispherical particles and an array of semi-conical structures (**Figure 2c,d and Figure 2 f,g)**. It is apparent that the optimal packing density is somewhere in between the close hexagonal packing and sparse random packing arrangements.

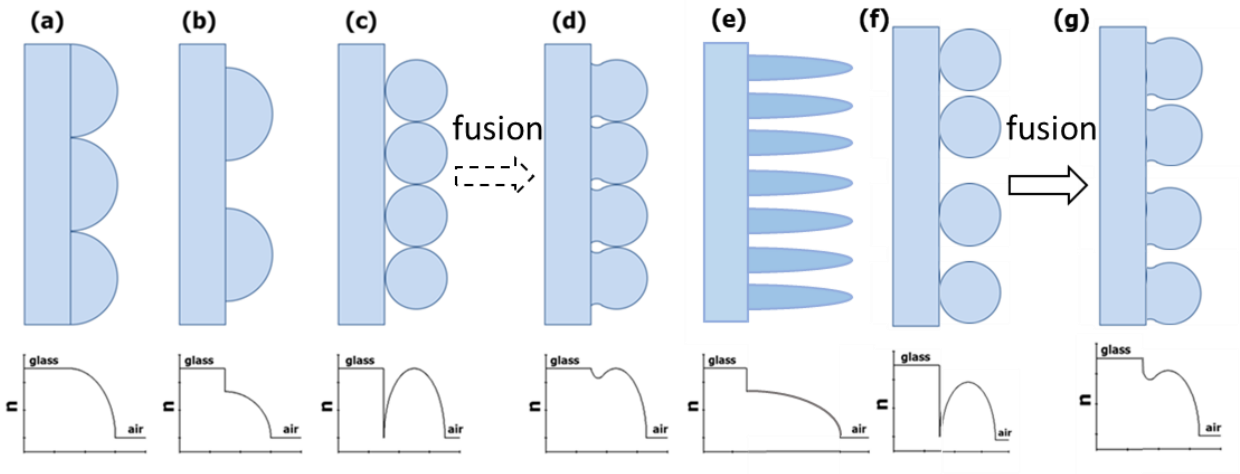

Figure 2. Schematic representation of feature arrangments and the corresponding average refractive index profiles of (a) array of tightly packed hemispheres; (b) array of sparsely packed hemispheres; (c) array of tightly packed spherical particles; (d) array of tightly packed spherical particles fused to the substrate when the layer structure resembles the hemispherical structure as shown in (a); (e) submicron structures mimicking moth's eye; and (f) and (g) microstructures generated in experiments (g) via random deposition of spherical particles (f) followed by hydrothermal fusion to the substrate.

We performed numerical modeling of optical properties of the silica nanoparticle coatings of different morphologies on the glass surface by varying the coating characteristics that could be reproduced in our experiments (**Figure 3**). These types of structures were simulated previously`.[34-35] However, we tailored this analysis to target characteristic dimensions and optical properties of materials used in our experiments. The spectral shape of the reflectance in the wavelength range of 350-2250 nm and average reflectance in the visible range (Rvis) were estimated using the Essential Macleod software package (Figure S1). This model does not account for scattering effects. Therefore, our calculations were applied for the particle diameter or the height of silica features (h) on the glass surface no greater than 200 nm. First, we found the optimal surface

coverage for minimal Rvis of a monolayer of hemispherical particles by analyzing the reflectance in a range of surface coverages from 60% - a random sequential addition (RSA), to 90% - a densely packed hexagonal 2D-lattice. The results proved that the optimal surface coverage of hemispheres lies between these two values (**Figure 3a 1-3**). Here, we demonstrate here the results for the 70% surface coverage because it is the greatest coverage achieved in our experiments, as discussed below. The 70% coverage is more efficient in minimizing the reflectance for larger structures and makes the reflectance less sensitive to the variation of size *h*. The latter result is practically important because nanoparticles are characterized by some polydispersity. Hydrothermal fusion may lead to further broadening of particle polydispersity due to the nonuniform thermal field and mass transport in the heterogeneous process as well as the dependence of the fusion rate on a particle size.

The results were compared with a uniform single layer coating of 51% porosity and a monolayer of spherical particles. The graphs in **Figure 3a** and **Figure 3b** demonstrate the advantages of hemispherical structures in terms of a better performance in a broad range of wavelengths and angles of incidence. From the results, an optimal height *h* is 107 nm for single layer uniform coating, 105 nm for spheres, and 150 nm for hemispheres. This result is important for the proper selection of silica particle size. We note that 150 nm feature height is also preferred from a process point of view, because of the tendency of nanoparticles to aggregate for sizes below 100 nm.

For the optimal h and the 70 % surface coverage, we compare the coatings consisting of hemispherical and spherical particles vs. the uniform single layer coating of the 51% porosity (**Figure 3c**). The results clearly demonstrate the advantage of hemispherical particles for the spectral width of the low reflectance region. The angular dependence of the reflectance for the best experimentally realized structure (*h*=150 nm, coverage 70%) of the hemispherical particle coating is shown in **Figure 3d**.

It has to be noted that the effect of particle polydispersity on AR properties of the coatings was not studied in this work in either experiment or numerical simulations. It seems clear that further broadening of polydispersity will change both the surface coverage and dimensions of the surface structures. Based on the results presented in Figure 3a, we may speculate that the broadening of polydispersity beyond 10% will increase the surface coverage but may not necessarily improve AR properties because the 70% coverage is close to the optimal coverage for *h*=150 nm.

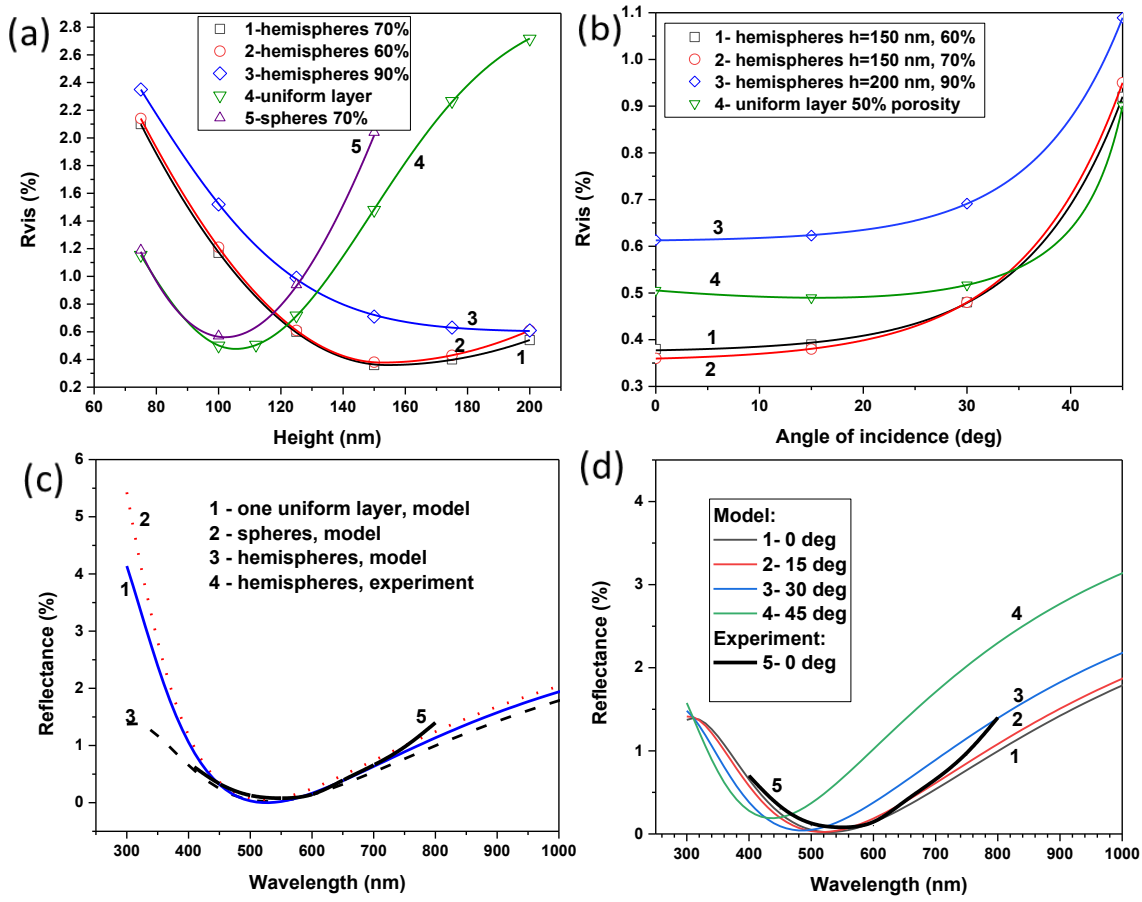

Figure 3. Numerical modeling results for the reflectance of silica coatings on glass for different structures and characteristic dimensions: (a) reflection vs. feature height *h*, comprising: 1- hemispheres at 70% surface coverage, 2- hemispheres at 60% surface coverage, 3- hemispheres at 90% surface coverage, 4- single layer coating with 51% porosity, and 5- spheres at 70% surface coverage; (b) angular dependence of Rvis for: 1- hemispheres at 60% surface coverage, *h*=150 nm, 2- hemispheres at 70% surface coverage, *h*=150 nm, 3- hemispheres at 90% surface coverage, *h*=200 nm, and 4- sinle layer coating with 51% porosity; (c) reflectance at the optimal *h* for: 1- uniform porous (51%) 107 nm thick single layer coating, 2- monolayer of 105 nm in diameter spherical particles at 70% coverage, 3 - 150 nm thick monolayer of hemispherical particles at 70% coverage, and 4- experimental results; (d) angular dependence of Rvis for the 150 nm thick monolayer of hemispherical particles at 70% coverage, 1, 2, 3, and 4 – for the angle of incidence of 0, 15, 30 and 45 degree, respectively, and 5- experimental results for the zero angle of incidence.

Fabrication of the AR-coating.

Based on the models and analysis, 200 nm silica particles were used to deposit a monolayer coating for hydrothermal annealing. This size was selected with the understanding that hydrothermal fusion will result in a decrease in the height of the structures generated on the glass to h< 200 nm.

The major challenge for the fabrication of a monolayer of nanoparticles is to generate a defectless, densely packed coating with 70% surface coverage. Possible defects are multilayers (particles deposited on top of already adsorbed particles), particle aggregates, and large gaps between adsorbed particles. Particle aggregates and larger gaps cause light scattering, decreasing the quality of the optical coating.

One of the commonly used approaches to describe the process of depositing a monolayer of spherical hard particles on the glass surface is a model of a random sequential addition (RSA). In this model, hard spheres sequentially, randomly, and irreversibly adsorb on the surface without overlap. At saturation, no space is available for other spheres. Numerical simulations for the RSA model predict the value of 0.547 for surface coverage by a monolayer of monodisperse particles.[36] The surface coverage can be progressively larger for polydisperse particles. For example, for a Gaussian distribution of particles by size with a standard deviation σ, the surface coverage θ can be approximated by the relationship: $\theta = 0.547 + 0.53\ \sigma$.[37] For a 10% standard deviation, the surface coverage could reach 0.60. However, particle-particle interactions in a colloidal dispersion are made repulsive to avoid particle aggregation. For a typical colloidal system with repulsively interacting particles, the RSA model predicts an even lower surface coverage. Therefore, the closely packed particle monolayer could be deposited at increased particle polydispersity and minimal interparticle repulsion. However, for the case of AR-coatings, the use of particles with a broad size distribution will causre a deviation from optimal layer characteristics and impair AR performance (Figure 3a).

In contrast with the RSA process, the highest theoretical density $\theta = 0.9069$ for monodisperse spherical particles in a 2D-lattice could be approached for the hexagonal packing arrangement. However, it is an extremely difficult task to fabricate highly ordered particle structures on large-area surfaces using existing scalable deposition methods. Furthermore, as the modeling results suggest (see Figures 3a and b), the closely packed hexagonal arrangement leads to significant degradation of the AR properties. On the other hand, the saturation limit for the RSA value of 0.547 is too low to approach the optimal optical properties and avoid the formation of light scattering gaps in the coating. For solving this challenge, the strategy in this work is to look for approaches that combine balancing particle-particle electrostatic interactions and exploring attractive capillary forces to form more closely packed 2D structures.[38] The process is realized on a pretreated glass substrate, providing a uniform electrostatic surface charge distribution. These mechanisms are used to overcome the RSA-process limitation for particle packing density.

An LbL assembly method was used to prepare an anchoring layer on the glass surface for the deposition of silica nanoparticles. This anchoring layer consists of 7 alternating layers of

oppositely charged polyelectrolytes PDDA and PSS and a top PDDA layer. This number of layers was found to be optimal based on the experiments. Such a combination provides a uniform positively charged anchoring surface of the glass, as discussed below. Negatively charged silica nanoparticles are attracted to the topmost positively charged PDDA polycation layer. The adsorbed particles exhibit a repulsive interaction with the particles in solution, thus preventing the formation of multilayers. However, these repulsive interactions limit the adsorption of particles in close proximity to each other. The higher the density of deposited particles, the stronger is a barrier for the deposition of another particle into the gap between the neighboring particles on the surface. Adsorption kinetics slows down substantially as the surface coverage increases, and the resulting coating is formed by sparsely deposited particles in good agreement with the RSA model and the experiments[39]. Since an optimal packing of deposited particles is a crucial factor in achieving improved optical characteristics, it is essential to address the factors that affect the adsorption kinetics, surface charge density, and its uniform distribution over the glass surface.

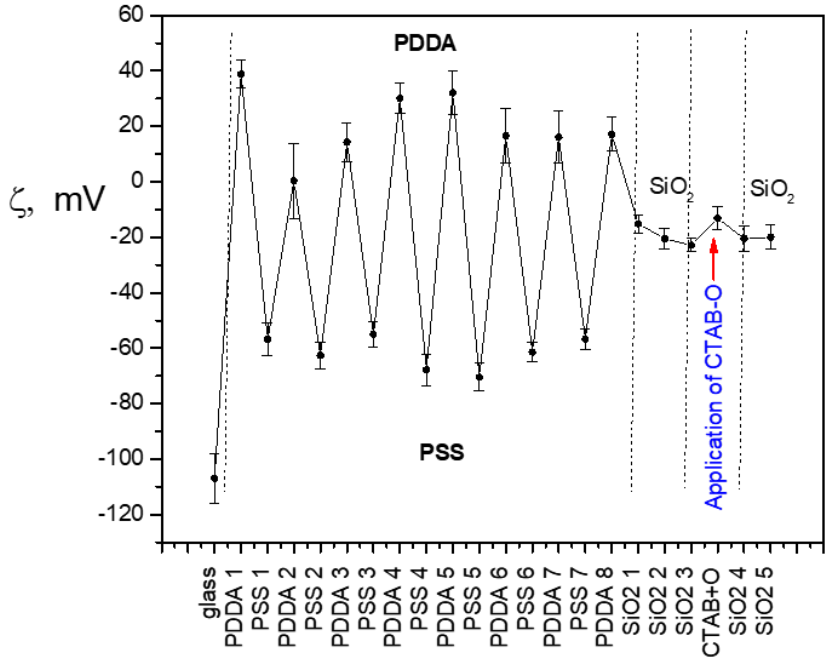

Figure 4. Zeta-potential after each deposition step: 7 layers of PDDA/PSS, 8th layer of PDDA, and 5 dip-rinse cycles of SiO_2 nanoparticles. After the deposition steps of silica particles, the surface was treated with a CTAB-octanol solution (shown with an arrow in the graph).

Measurements of the Zeta-potential of the glass surface in the sodium chloride electrolyte solution were used to monitor surface charge after each step of LbL polyelectrolyte deposition **(Figure 4**). The clean alkali aluminosilicate glass is negatively charged ($\zeta = -105$ mV). Each time after the deposition of PDDA or PSS, the Zeta-potential is switched from a positive to a negative value.

Strong oscillations of Zeta-potential values for the initial five layers is likely due to a nonuniform charge distribution on the surface. After six depositions of PSS and PDDA polyelectrolytes, the Zeta-potential stabilizes with minimal variations.

Spherical silica particles were deposited following the deposition of PSS-PDDA in several consecutive steps. The deposition of silica particles on the LbL anchoring layer with less than 6 PSS-PDDA sublayers yields coatings with a low surface coverage (**Figure 5a).** A much greater coverage was approached for the particle deposition on the anchoring layers consisting of 7 polyelectrolyte layers plus PDDA on top. The first deposition of silica particles results in the surface coverage of 0.58±0.05 (**Figure 5**b), in a good agreement with the RSA model. Each step of the deposition of silica particles leads to a more negative value of the Zeta-potential (**Figure 4**). The built-up of a negative charge delays the adsorption of particles preserving a large fraction of uncovered areas. It was demonstrated elsewhere that an increase of the ionic strength could be used to screen interparticle electrostatic repulsion to increase the surface coverage.[39] However, any attempt to increase the ionic strength of the silica nanoparticle solutions resulted in some particle aggregation and deposition of 3D-aggregates. These aggregates, being present on the surface even in a small fraction, cause an unacceptable level of light scattering.

A selective cancelation of electrostatic repulsion between the deposited particles and the particles in dispersion was achieved by the treatment of the coating with a CTAB-n-octanol (CTAB-O) mixture. The mechanism of the CTAB-O effect is schematically explained in **Figure 6**. CTAB is a cationic surfactant that binds to acidic silanol groups on the silica surface. n-Octanol is a co-surfactant minimizing hydrophobization of silica particles by forming a hydrophobic complex (**Figure 6**a). The CTAB-O treatment is applied to the particles in the coating, while particles in the dispersions remain electrostatically stabilized. Thus, the CTAB-O complex is only formed on the surface of silica particles residing on the glass substrate. This treatment results in a decrease of the negative charge on the coated surface, as concluded from the Zeta-potential measurements (**Figure 4**). In the following deposition step, the surface charge of silica particles in the colloidal dispersion remains unchanged, while the particles in the coating are less charged. Consequently, the repulsive barrier for adsorption of newly arriving silica particles from the solution becomes lower **(Figure 6b**). Following this step, the Zeta-potential becomes more negative, indicating an additional deposition of silica particles after CTAB-O treatment of the coating (**Figure 4**). The analysis of SEM images provides evidence of higher surface coverage (**Figure 5 c,d**).

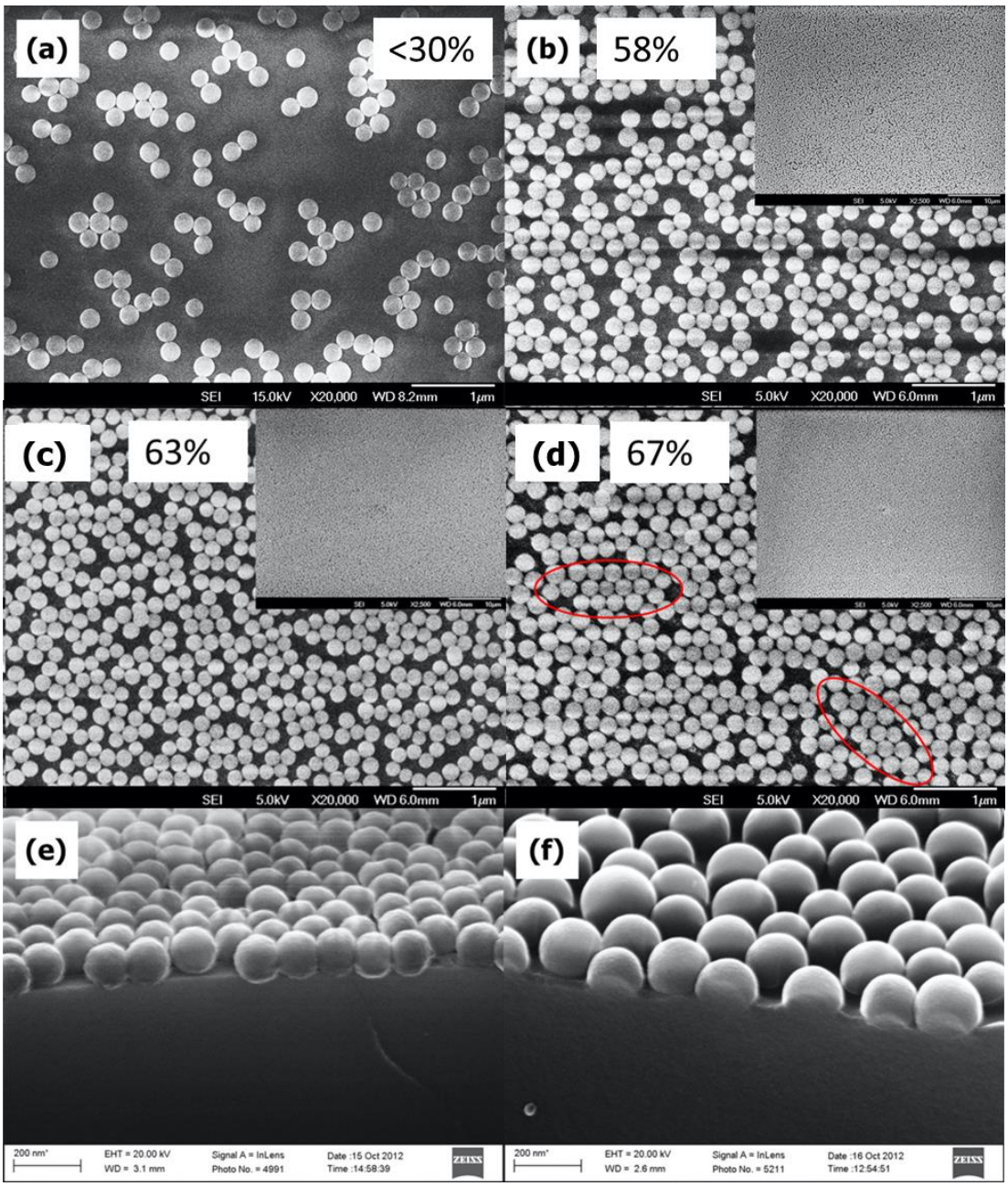

Figure 5. SEM images of silica particles deposited on the alkali aluminosilicate glass substrate by spray deposition: (a) A typical coverage for deposited silica particles at a low concentration of particles in the dispersion (<30% coverage); (b) $(PDDA\text{-}PSS)_7PDDA$ (1 cycle of SiO_2) - the substrate modified with 7PDDA/PSS +1 PDDA layers and with 1 cycle of silica particles deposition prepared (53% coverage); (c) $(PDDA\text{-}PSS)_7PDDA$ (2 cycles of SiO_2/Octanol-CTAB/2 cycles of SiO_2), 63% coverage; (d) $(PDDA\text{-}PSS)_7PDDA$ (3 cycles of SiO_2/Octanol-CTAB/2 cycles of SiO_2), 67% coverage; (e) 150 nm silica particles coatings and (f) 200 nm particles after hydrothermal fusion. The insets show larger of 50x50 μm^2 areas. The surface coverage values are calculated from collections of in-plane SEM images for each sample.

A close examination reveals a tendency of deposited particles to form closely packed 2D-aggregates on the surface. It is likely that silica particles are not strongly bound to the polyelectrolyte anchoring layer and can be transported on the surface by attractive capillary forces in the coating while drying. The capillary forces overcome electrostatic repulsion and form closely packed domains with the hexagonal arrangement of the particles (**Figure 5d**) in agreement with the well-known mechanism of the two-dimensional ordering of fine particles due to the menisci formed around the particles.[38] The fraction of these ordered domains increases with each cycle of particle adsorption, followed by drying for both the dip-rinse (**Figure S5**) and spray deposition (**Figure 5** and **Figure S6**) methods.

The spray-deposition method demonstrated a 4% lower surface coverage as compared with dip-rinse. The detailed study of the coatings revealed areas of closely packed particles with defects in between. The number of defects decreases with a number of deposition cycles and optimization of spray-deposition conditions: nozzle size, air pressure, working distance, etc. (**Table S1, Figure S7**).

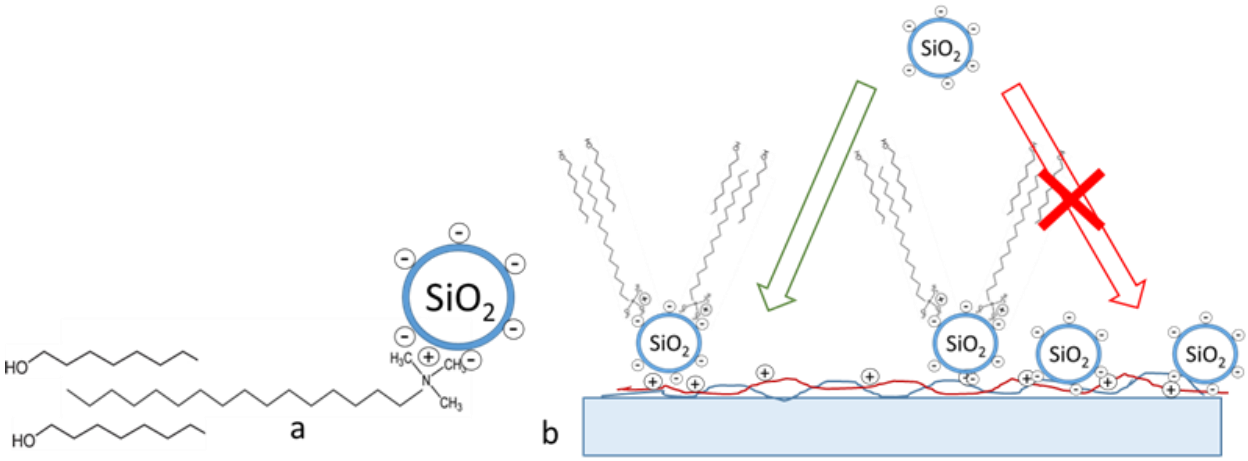

Figure 6. Schematic for the mechanism of an increased surface coverage due to the application of CTAB-O (see the discussion in the text): (a) formation of an electrolyte and hydrophobic complex that results in a decrease of the surface charge of silica particles residing on the glass surface; (b) adsorption of silica particles from a solution on the vacant sites with lower repulsive interactions exerted by neighboring adsorbed particles.

A combination of both methods, the surface treatment with CTAB-O solutions and the repetition of deposition-drying cycles synergistically improve the surface coverage up to 0.7±0.03 for the dip-coating method and up to 0.66±0.03 for the spray-coating that exceeds the RSA limit of 0.6 for spherical particles with the 10% standard deviation by size (**Figure 7**).

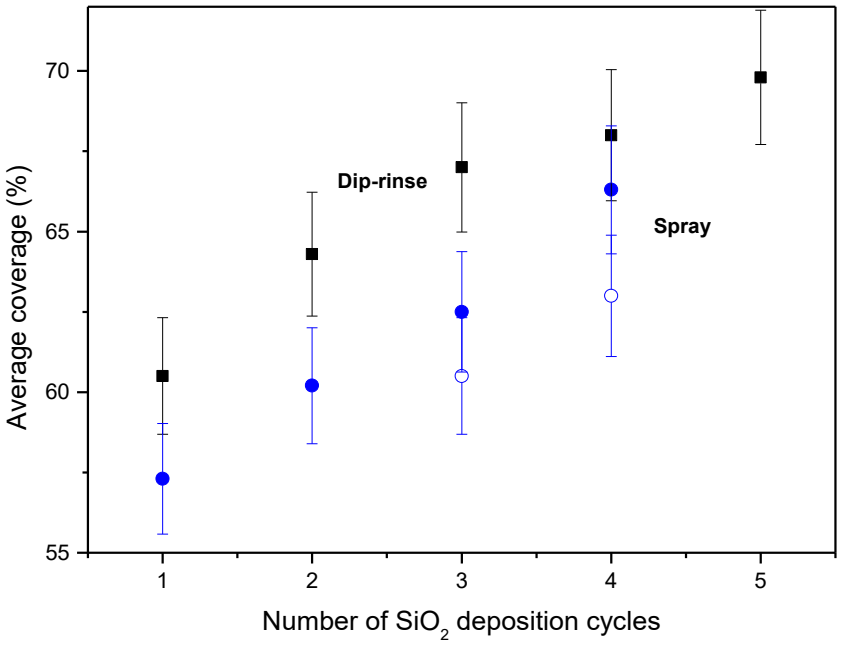

Figure 7. The average coverage was calculated from SEM images for dip-rinse (square) and spray-coating (circle) methods versus a number of SiO_2 deposition cycles. Solid symbols correspond to substrates that were treated with a CTAB-O after 2-3 cycles of silica particle deposition. The open symbols correspond to spray-coated samples without a CTAB-O treatment.

The prepared samples with a closely packed monolayer of silica particles were annealed in a steam furnace. **Figure 5e,f** demonstrate representative SEM images of silica particle monolayers on the glass substrates before and after fusion. Since the modeling suggests the 150 nm optimal height of the structure, we compare the SEM images of a monolayer of 150 nm diameter spherical particle (Figure 5e) and a monolayer of 200 nm particles partially fused to the glass substrate (Figure 5f). From the comparison, the difference between the two structures is apparent: due to the fusion 200 nm particles increase their contact area with the substrate to almost the full diameter and become shorter in the vertical direction (about 150 nm remaining height).

During the hydrothermal annealing, the deposited silica particles fuse with the glass substrate underneath. The mechanism of this process is a combination of materials' diffusions and Ostwald ripening when nanoparticles residing on the glass surfaces in high-temperature humid conditions change their shape through the dissolution-condensation mechanism and form covalent bonds that bind the particle and glass substrate. The particle shape is changing via the formation of a bridging "neck". This process is driven by a decrease in the free surface energy. It was shown experimentally that the adhesion force between the particle and the substrate is equivalent to the

yield stress of glass.[40] The mechanism of dissolution and condensation is described by the chemical reaction

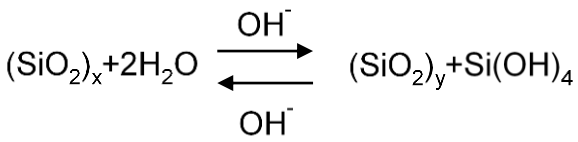

with the highest rates in both directions at a pH range close to the neutral pH.[41] The rate of fusion increases at neutral pH in the presence of polyamines[42] and with an increase of temperature. In our case, PDDA might have catalyzed the dissolution-precipitation process of the silica particles fusion to the glass substrate for 1 h at 100% humidity at 600 ºC in the initial stages of the fusion process prior to pyrolysis of the polyelectrolytes. The coating is transformed from a monolayer of closely packed spherical particles into a monolayer of closely packed nearly hemispherical particles (Figure 2g) that resemble a moth-eye structure.

Characterization of the coatings

Transmission spectra for the coatings before and after the fusion of silica nanoparticles are shown in **Figure 8**. Before fusion, the spectra of the coated glass show better transparency than the reference uncoated glass sample only for longer wavelength (**Figure 8a,b)**. The observed reduction of transparency for the violet-blue part of the spectrum is primarily due to a non-gradual change of refractive index at the substrate-particle interface (**Figure 2c,f**). Since the presented samples were fabricated by deposition of 200 nm SiO_2 particles, the light scattering is also observed primarily at a shorter wavelength.

The analysis of the samples prior to the hydrothermal treatment after each cycle of the particle deposition reveals that each additional SiO_2 deposition step improves optical properties and shifts the spectra towards higher values of transparency (**Figure 8a**). These results are in agreement with the surface coverage data (**Figure 7**).

Similar tendencies are observed for transmission spectra of the samples prepared using both dip-rinse and spray-coating methods. Since spray-deposited coatings demonstrated a lower surface coverage, the transparency of these samples is inferior to the dip-rinse coated glasses. However, an interesting effect was found for a combination of a spray-coating (4 cycles of SiO_2 deposition) with one dip-rinse cycle. The achieved transparency is better than that for a sample with five cycles of dip-rinse deposited particles, although the estimated coverage for both samples was similar. It is possible that a combination of both dip-rinse and spray methods can be used for optimization to

target better optical performance due to the minimized number of light scattering defects in the structures.

The spectra for the hydrothermally treated samples were measured for substrates modified on one side only. After the hydrothermal annealing, the thickness of the coating becomes lower, and the change of the refractive index from air to glass is closure to a graded index case. This results in improved optical transparency, and a decreased reflectance with a reflectance minimum shifted to a shorter wavelength for samples with a higher degree of particle fusion (**Figure 8c**). The measured values of reflectance are 0.8, 0.1, and 0.7% ± 0.05% at 450, 550, and 650 nm wavelength, respectively. The results are in good agreement with modeling (**Figure 3d**).

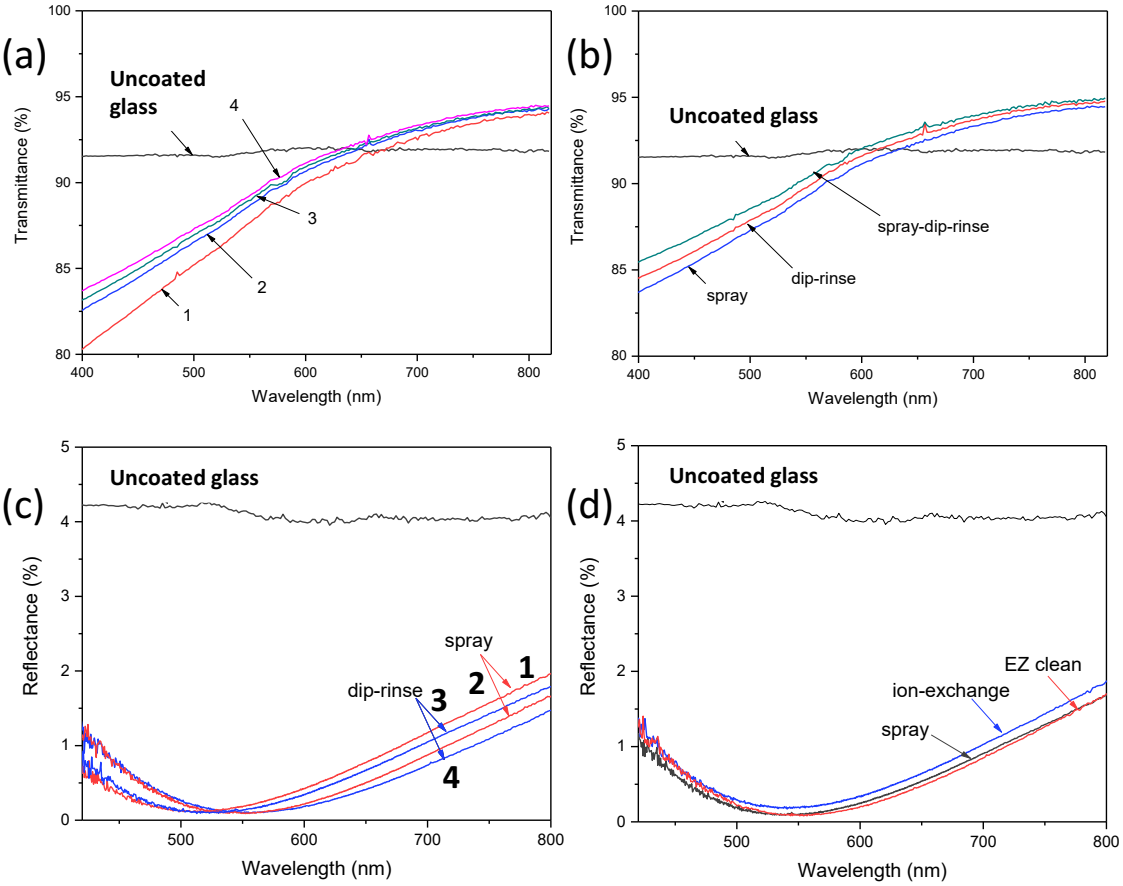

Figure 8. (a) Transmission spectra of spray-coated substrates after each step of the modification. The numbers correspond to the numbers of SiO_2 deposition cycles. (b) Transmission spectra of dip-rinse and spray-coated substrates before the fusion of silica particles. (dip-rinse) five cycles of dip-rinse deposition; (spray) four cycles of spray deposition; (spray-dip-rinse) four cycles of spray deposition and one cycle of dip-rinse deposition. (c) Reflectance spectra of dip-rinse and spray-coated substrates after fusion of silica particles. Two series of dip-rinse and spray-coated samples are presented with different degree of particle fusion to the substrate (for curves 2 and 4 a degree

of fusion is greater than for 1 and 3, controlled by annealing time 30 min and 1 h) and reflection minima at about 550 and 510 nm, respectively. (d) Reflectance spectra of the fused sprayed sample before and after the ion-exchange process and hydrophobic/oleophobic functionalization by a PFPE silane solution.

Some deviation of the model from the experimental result at longer wavelengths can be explained by at least two structural differences. First, the model was developed for the hemispherical structures, while the fusion process results in more complex geometry (**Figure 5f**). Second, the model considers a laterally uniform optical layer. In the experiments, we observe a combination of domains with hexagonal packing and sparse areas of particle deposition (**Figure 5d**), leading to some light scattering.

The measured haze values for dip-rinse and spray-coated substrates are 2.4 and 2.5% ± 0.1%, respectively. After additional modification by the ion-exchange process and hydrophobic/oleophobic surface treatment (deposition of fluorosilanes), the optical properties were measured again (**Figure 8d**). The reflectance spectrum after the ion-exchange process demonstrates no substantial changes; the haze is decreased to the value of 1.8±0.1%. After functionalization with fluorosilane, the resulting optical characteristics were not changed.

Table 1. Mechanical and chemical resistance of the AR-coatings

Treatment	Characteristics after the treatment	
	Average reflectance,% ±0.2%	Visual defects
550 ^{0}C, 100% humidity, 1 h	0.5	No
400 ^{0}C molten potassium salt bath, 1h	0.5	No
15% HCl, room temperature, 1 h	0.5	No
Tissue wiping with a surfactant solution	0.5	No
Organic solvents (ethanol, acetone, toluene)	0.5	No
Pencil scratch test H-6H	0.5	No
Steel wool scratch test	NA*	Appearance of scratches

*Increased scattering

Mechanical testing was conducted using pencils of various hardness (up to 6H). The tests revealed no damage to the coating. The surface structure was analyzed by SEM and optical microscopy. No scratches were detected, and no visual defects were observed after testing with 4H-6H pencils. The softer pencils occasionally left traces of graphite particles, but no structural damage to the coating

was observed (**Figure S9b**). The steel wool tests show that the coating structure is damaged and scratches become visible with an optical microscope (**Figure S9c**). The results of mechanical and chemical tests show very good mechanical stability and scratch resistance sufficient for many applications when no hard abrasives are involved (**Table 1**).

Self-cleaning antireflective coatings

A number of applications, such as touch screens, windows, and solar panels, can benefit from additional self-cleaning properties at atmospheric conditions. A common approach to create superhydrophobic/oleophobic coatings which secure stain-resistant and self-cleaning properties is to engineer re-entrant structures with a low surface energy[43]. A 2D-monolayer of spherical particles is one of the examples of the re-entrant surface, which becomes non-wettable if the particle surface is modified with low-surface energy materials. However, the breakthrough pressure for such structures is low[44]. After hydrothermal annealing, the shape of particles changes to hemispherical with the loss of the re-entrant geometry.

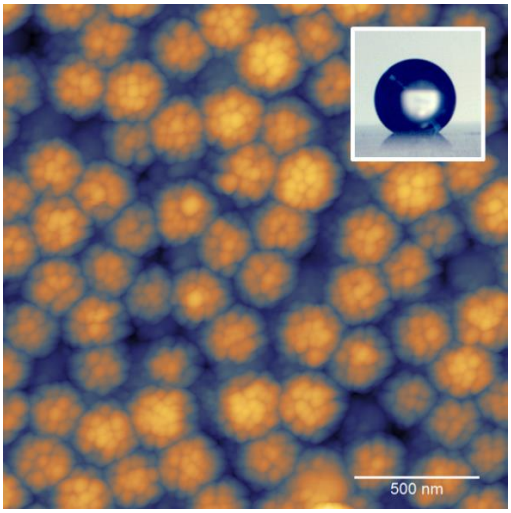

Figure 9. AFM image of the superhydrophobic coating obtained by additional spray coating with 20-30 nm silica particles with subsequent fluorosilane hydrophobization. The inset presents an optical image of a water drop on the coating.

The non-wetting property of spherical particle coatings is typically improved by the generation of raspberry-type structures when the particles in the coating are coated with nanoparticles smaller by size, which adds re-entrant structures at a smaller scale. In this work, 25 nm silica particles were deposited using a spray deposition method. After that, the coating was functionalized with fluorosilane to minimize the surface energy. The morphology of the coating is shown in **Figure 9**. The coating is non-wettable, with a water contact angle of 150° ± 5 °. This additional layer of

smaller nanoparticles has a minimal effect on the transparency of the sample with the average transparency reduced by less than 1% for 2-side coatings (**Figure S10**).

Summary

Transparent and robust all-nanoparticle antireflective coatings made of closely packed monolayers of hemispherical silica particles were formed on glass substrates. The coatings were assembled by multiple depositions of 200 nm spherical silica particles on the LbL polyelectrolyte anchoring layers, which modified the glass surface with uniformly distributed positive surface charges by dip-rinse or spray-coating methods. Multiple depositions (3-4) of silica particles yielded a surface coverage of about 0.6. This was followed by the application of cationic and nonionic surfactants CTAB and n-octanol to further modify the surface of the coating and reduce electrostatic repulsions between silica nanoparticles while securing the colloidal stability of the particle dispersions. The resulting surface coverage approached 0.7, which is substantially greater than that observed for the random sequential addition process in simulations and experiments (0.547 and 0.6 for monodisperse particles and polydisperse particles with a standard deviation by size of 10%, respectively).

The coating was annealed in a superheated steam atmosphere to induce a hydrothermal annealing process similar to Ostwald ripening. The particles were transformed from spherical to hemispherical shape and fused to the glass substrate. The 2D-hemispherical densely packed nanoparticle layer provided a gradual change of a refractive index at the glass-air interface. The spectroscopic analysis revealed the minimum and average reflectance of 0.1% and 0.5%, respectively, in the visible wavelength range, in good agreement with numerical models. The hydrothermal annealing improved the mechanical integrity of the coating and its scratch resistance up to the 6H pencil hardness level.

The coatings were fabricated using two scalable deposition methods: dip-rinse and spray-rinse, by alternating deposition of particles by immersing the glass in the particle dispersion or spraying it on the glass surface, respectively, and followed up by rinsing and drying of the coated glass. The optical characteristics of the coatings prepared by these two methods were quite similar, while the spray-coated samples were a little lower in transparency as compared with the dip-rinse coated ones. However, the best result was demonstrated for a combination of these two methods (spray-coating first and dip-rinse as the last deposition step).

The improved transparency of the particle coatings correlated directly with the surface coverage. The experiments performed to develop the coating method demonstrated that multiple deposition-rinsing steps followed by sample drying are critical to employ attractive capillary forces and generate closely packed nanoparticle domains in the coatings. The latter, if combined with suppressing electrostatic repulsion between particles in the coating and particles in suspension, resulted in densely packed particle layers with a surface coverage of 0.7 and no 3D-aggregates. This mechanism can be realized if the particle-glass interaction is strong but reversible when particles can be transported on the surface under the action of capillary forces.

Additional deposition of smaller particles (25 nm) functionalized with fluorosilane on the surface of the antireflective coating was used to fabricate superhydrophobic surfaces characterized with a water contact angle of 150° ± 5°, while optical properties were not significantly affected by this modification. Such a method is a scalable approach to the fabrication of durable transparent antireflective coatings for various applications.

ASSOCIATED CONTENT

Supporting Information. Supporting Information is available free of charge at…

Protocols for dip-rinse and spray deposition, processing of SEM images, estimation of Z-potential of the coatings, surface coverage for spray coatings, optimization of spray-coating parameters, the effect of deposition cycles on the surface coverage, pencil scratch tests of the coatings, and transmission spectra after deposition of 25 nm particles on top of the coating.

Video1. Example of manual pencil scratch test.

AUTHOR INFORMATION

Corresponding Authors

*E-mail: KuksenkoDV@Corning.com

*E-mail: sminko@uga.edu (S.M.). Tel: 7065423122, Fax: 7065420410.

ACKNOWLEDGMENT

Thi work was supported by Corning Incorporated and, in part, by NSF awards DMR 1904365.

REFERENCES

(1) Raut, H. K.; Ganesh, V. A.; Nair, A. S.; Ramakrishna, S. Antireflective Coatings: a Critical, In-Depth Review. *Energy Environ. Sci.* **2011,** *4* (10), 3779-3804, DOI: 10.1039/C1ee01297e.

(2) Li, X.; Yu, X. H.; Han, Y. C. Polymer Thin Films For Antireflection Coatings. *J. Mater. Chem. C* **2013,** *1* (12), 2266-2285, DOI: 10.1039/C2tc00529h.

(3) Buskens, P.; Burghoorn, M.; Mourad, M. C. D.; Vroon, Z. Antireflective Coatings For Glass And Transparent Polymers. *Langmuir* **2016,** *32* (27), 6781-6793, DOI: 10.1021/Acs.Langmuir.6b00428.

(4) Chattopadhyay, S.; Huang, Y. F.; Jen, Y. J.; Ganguly, A.; Chen, K. H.; Chen, L. C. Anti-Reflecting and Photonic Nanostructures. *Mater. Sci. Eng. R Rep.* **2010,** *69* (1-3), 1-35, DOI: 10.1016/J.Mser.2010.04.001.

(5) Yao, L.; He, J. H. Recent Progress in Antireflection And Self-Cleaning Technology - From Surface Engineering to Functional Surfaces. *Prog. Mater. Sci.* **2014,** *61*, 94-143, DOI: 10.1016/J.Pmatsci.2013.12.003.

(6) Hedayati, M. K.; Elbahri, M. Antireflective Coatings: Conventional Stacking Layers and Ultrathin Plasmonic Metasurfaces, A Mini-Review. *Materials* **2016,** *9* (6), DOI: 10.3390/Ma9060497.

(7) Ye, L. Q.; Zhang, S. M.; Wang, Q.; Yan, L. H.; Lv, H. B.; Jiang, B. Mechanically Stable Single-Layer Mesoporous Silica Antireflective Coating on Solar Glass. *RSC Adv.* **2014,** *4* (67), 35818-35822, DOI: 10.1039/C4ra05309e.

(8) Du, X.; Xing, Y.; Zhou, M. Y.; Li, X. Y.; Huang, H. W.; Meng, X. M.; Wen, Y. Q.; Zhang, X. J. Broadband Antireflective Superhydrophilic Antifogging Nano-Coatings Based on Three-Layer System. *Microporous Mesoporous Mater.* **2018,** *255*, 84-93, DOI: 10.1016/J.Micromeso.2017.07.017.

(9) Adv. Mater. Miamiao, L.; Su, L. F.; Tanemura, S.; Fisher, C. A. J.; Zhao, L. L.; Liang, Q.; Xu, G. Cost-Effective Nanoporous Sio2-Tio2 Coatings on Glass Substrates With Antireflective and Self-Cleaning Properties. *Appl. Energy* **2013,** *112*, 1198-1205, DOI: 10.1016/J.Apenergy.2013.03.043.

(10) Wang, X. D.; Shen, J. Sol-Gel Derived Durable Antireflective Coating for Solar Glass. *J. Sol-Gel Sci. Technol.* **2010,** *53* (2), 322-327, DOI: 10.1007/S10971-009-2095-Y.

(11) Ye, L. Q.; Zhang, Y. L.; Zhang, X. X.; Hu, T.; Ji, R.; Ding, B.; Jiang, B. Sol-Gel Preparation of SiO2/TiO2/SiO2-TiO2 Broadband Antireflective Coating for Solar Cell Cover Glass. *Sol. Energy Mater. Sol. Cells* **2013,** *111*, 160-164, DOI: 10.1016/J.Solmat.2012.12.037.

(12) Li, X. G.; Shen, J. A Scratch-Resistant And Hydrophobic Broadband Antireflective Coating by Sol-Gel Method. *Thin Solid Films* **2011,** *519* (19), 6236-6240, DOI: 10.1016/J.Tsf.2011.03.114.

(13) Gombert, A.; Glaubitt, W.; Rose, K.; Dreibholz, J.; Blasi, B.; Heinzel, A.; Sporn, D.; Doll, W.; Wittwer, V. Subwavelength-Structured Antireflective Surfaces on Glass. *Thin Solid Films* **1999,** *351* (1-2), 73-78, DOI: 10.1016/S0040-6090(98)01780-5.

(14) Clapham, P. B.; Hutley, M. C. Reduction of Lens Reflection by Moth Eye Principle. *Nature* **1973,** *244* (5414), 281-282, DOI: 10.1038/244281a0.

(15) Mazumder, P.; Jiang, Y. D.; Baker, D.; Carrilero, A.; Tulli, D.; Infante, D.; Hunt, A. T.; Pruneri, V. Superomniphobic, Transparent, and Antireflection Surfaces Based on Hierarchical Nanostructures. *Nano Lett.* **2014,** *14* (8), 4677-4681, DOI: 10.1021/Nl501767j.

(16) Ji, S.; Song, K.; Nguyen, T. B.; Kim, N.; Lim, H. Optimal Moth Eye Nanostructure Array on Transparent Glass Towards Broadband Antireflection. *ACS Appl. Mater. Interfaces* **2013,** *5* (21), 10731-10737, DOI: 10.1021/Am402881x.

(17) Rombaut, J.; Maniyara, R. A.; Bellman, R. A.; Acquard, D. F.; Baca, A. S.; Osmond, J.; Senaratne, W.; Quesada, M. A.; Baker, D.; Mazumder, P.; Pruneri, V. Antireflective Transparent Oleophobic Surfaces By Noninteracting Cavities. *ACS Appl. Mater. Interfaces* **2018,** *10* (49), 43230-43235, DOI: 10.1021/Acsami.8b15507.

(18) Min, W. L.; Jiang, B.; Jiang, P. Bioinspired Self-Cleaning Antireflection Coatings. *Adv. Mater.* **2008,** *20* (20), 3914-3918, DOI: 10.1002/Adma.200800791.

(19) Trespidi, F.; Timo, G.; Galeotti, F.; Pasini, M. PDMS Antireflection Nano-Coating for Glass Substrates. *Microelectron. Eng.* **2014,** *126*, 13-18, DOI: 10.1016/J.Mee.2014.03.043.

(20) Galeotti, F.; Trespidi, F.; Timo, G.; Pasini, M. Broadband and Crack-Free Antireflection Coatings by Self-Assembled Moth Eye Patterns. *ACS Appl. Mater. Interfaces* **2014,** *6* (8), 5827-5834, DOI: 10.1021/Am500687f.

(21) Sun, J. Y.; Wang, X. B.; Wu, J. H.; Jiang, C.; Shen, J. J.; Cooper, M. A.; Zheng, X. T.; Liu, Y.; Yang, Z. G.; Wu, D. M. Biomimetic Moth-Eye Nanofabrication: Enhanced Antireflection with Superior Self-Cleaning Characteristic. *Sci. Rep.* **2018,** *8*, DOI: 10.1038/S41598-018-23771-Y.

(22) Liu, X. M.; He, J. H. Hierarchically Structured Superhydrophilic Coatings Fabricated by Self-Assembling Raspberry-Like Silica Nanospheres. *J. Colloid Interface Sci.* **2007,** *314* (1), 341-345, DOI: 10.1016/J.Jcis.2007.05.011.

(23) Li, X. Y.; He, J. H. In Situ Assembly of Raspberry- and Mulberry-Like Silica Nanospheres Toward Antireflective and Antifogging Coatings. *ACS Appl. Mater. Interfaces* **2012,** *4* (4), 2204-2211, DOI: 10.1021/Am3002082.

(24) Zhao, Y.; Wang, J. S.; Mao, G. Z. Colloidal Subwavelength Nanostructures for Antireflection Optical Coatings. *Opt. Lett.* **2005,** *30* (14), 1885-1887, DOI: 10.1364/Ol.30.001885.

(25) Xu, L. G.; He, J. H. Antifogging And Antireflection Coatings Fabricated by Integrating Solid and Mesoporous Silica Nanoparticles Without Any Post-Treatments. *ACS Appl. Mater. Interfaces* **2012,** *4* (6), 3293-3299, DOI: 10.1021/Am300658e.

(26) Tao, M.; Zhou, W. D.; Yang, H. J.; Chen, L. Surface Texturing by Solution Deposition for Omnidirectional Antireflection. *Appl. Phys. Lett.* **2007,** *91* (8), DOI: 10.1063/1.2775805.

(27) Ren, T. T.; Geng, Z.; He, J. H.; Zhang, X. J.; He, J. A Versatile Route to Polymer-Reinforced, Broadband Antireflective and Superhydrophobic Thin Films Without High-Temperature Treatment. *J. Colloid Interface Sci.* **2017,** *486*, 1-7, DOI: 10.1016/J.Jcis.2016.09.054.

(28) Ye, X.; Huang, J.; Zhang, J. C.; Jiang, X. D.; Wu, W. D.; Zheng, W. G. Subwavelength Porous Silica Antireflection Coating. *J. Optoelectron. Adv. Mater.* **2011,** *13* (5-6), 532-536.

(29) Zhi, J. H.; Zhang, L. Z. Durable Superhydrophobic Surface with Highly Antireflective and Self-Cleaning Properties for the Glass Covers of Solar Cells. *Appl. Surf. Sci.* **2018,** *454*, 239-248, DOI: 10.1016/J.Apsusc.2018.05.139.

(30) Ren, T. T.; He, J. H. Substrate-Versatile Approach to Robust Antireflective and Superhydrophobic Coatings with Excellent Self-Cleaning Property in Varied Environments. *ACS Appl. Mater. Interfaces* **2017,** *9* (39), 34367-34376, DOI: 10.1021/Acsami.7b11116.

(31) Ge, D. T.; Yang, L. L.; Zhang, Y. F.; Rahmawan, Y.; Yang, S. Transparent and Superamphiphobic Surfaces from One-Step Spray Coating of Stringed Silica Nanoparticle/Sol Solutions. *Part. Part. Syst. Charact.* **2014,** *31* (7), 763-770, DOI: 10.1002/Ppsc.201300382.

(32) Nogueira, G. M.; Banerjee, D.; Cohen, R. E.; Rubner, M. F. Spray-Layer-By-Layer Assembly Can More Rapidly Produce Optical-Quality Multistack Heterostructures. *Langmuir* **2011,** *27* (12), 7860-7867, DOI: 10.1021/La200790g.

(33) Aytug, T.; Lupini, A. R.; Jellison, G. E.; Joshi, P. C.; Ivanov, I. H.; Liu, T.; Wang, P.; Menon, R.; Trejo, R. M.; Lara-Curzio, E.; Hunter, S. R.; Simpson, J. T.; Paranthaman, M. P.; Christen, D. K. Monolithic Graded-Refractive-Index Glass-Based Antireflective Coatings: Broadband/Omnidirectional Light Harvesting and Self-Cleaning Characteristics. *J. Mater. Chem. C* **2015,** *3* (21), 5440-5449, DOI: 10.1039/C5tc00499c.

(34) Zhou, W.; Tao, M.; Chen, L.; Yang, H. Microstructured Surface Design for Omnidirectional Antireflection Coatings on Solar Cells. *J. Appl. Phys.* **2007,** *102* (10), DOI: 10.1063/1.2817470.

(35) Song, Y. M.; Choi, H. J.; Yu, J. S.; Lee, Y. T. Design of Highly Transparent Glasses with Broadband Antireflective Subwavelength Structures. *Opt. Express* **2010,** *18* (12), 13063-13071, DOI: 10.1364/Oe.18.013063.

(36) Zhang, G.; Torquato, S. Precise Algorithm to Generate Random Sequential Addition of Hard Hyperspheres at Saturation. *Phys. Rev. E* **2013,** *88* (5), Article Number: 053312 DOI: 10.1103/Physreve.88.053312.

(37) Adamczyk, Z.; Siwek, B.; Zembala, M.; Weronski, P. Influence of Polydispersity on Random Sequential Adsorption of Spherical Particles. *J. Colloid Interface Sci.* **1997,** *185* (1), 236-244, DOI: 10.1006/Jcis.1996.4540.

(38) Denkov, N. D.; Velev, O. D.; Kralchevsky, P. A.; Ivanov, I. B.; Yoshimura, H.; Nagayama, K. Mechanism of Formation of 2-Dimensional Crystals From Latex-Particles on Substrates. *Langmuir* **1992,** *8* (12), 3183-3190, DOI: 10.1021/La00048a054.

(39) Bohmer, M. R.; Van Der Zeeuw, E. A.; Koper, G. J. M. Kinetics of Particle Adsorption in Stagnation Point Flow Studied by Optical Reflectometry. *J. Colloid Interface Sci.* **1998,** *197* (2), 242-250, DOI: 10.1006/Jcis.1997.5236.

(40) Feng, J. W.; Busnaina, A. A.; Ryszytiwskyj, W. P. Effect of Humidity and Aging on Adhesion and Removal of Glass Particles from FPD Glass. *Surface Eng.* **2001,** *17* (5), 425-429, DOI: 10.1179/026708401101518015.

(41) Iller, R. K. *The Chemistry of Silica: Solubility, Polymerization, Colloid and Surface Properties and Biochemistry of Silica*, John Wiley & Sons: New York/Chichester/Brisbane/Toronto, 1979; P 866.

(42) Patwardhan, S. V.; Tilburey, G. E.; Perry, C. C. Interactions of Amines With Silicon Species in Undersaturated Solutions Leads to Dissolution and/or Precipitation of Silica. *Langmuir* **2011,** *27* (24), 15135-15145, DOI: 10.1021/La204180r.

(43) Valipour, M. N.; Birjandi, F. C.; Sargolzaei, J. Super-Non-Wettable Surfaces: A Review. *Colloids Surf. Physicochem. Eng. Asp.* **2014,** *448*, 93-106, DOI: 10.1016/J.Colsurfa.2014.02.016.

(44) Tuteja, A.; Choi, W.; Mabry, J. M.; Mckinley, G. H.; Cohen, R. E. Robust Omniphobic Surfaces. *Proc. Natl. Acad. Sci.* **2008,** *105* (47), 18200-18205, DOI: 10.1073/Pnas.0804872105.

TOC image

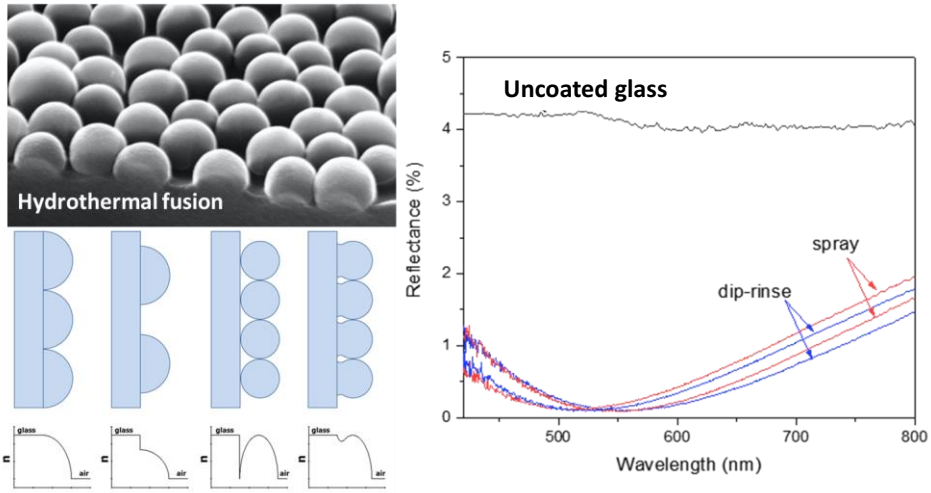
Hydrothermal fusion
glass
air
n
Uncoated glass
spray
dip-rinse
Reflectance (%)
Wavelength (nm)
0
1
2
3
4
5
500
600
700
800